Anal. Chem. **2009,** *81,* 2303–2310

Particle Trapping in High-Conductivity Media with Electrothermally Enhanced Negative Dielectrophoresis

Seungkyung Park, Mehti Koklu, and Ali Beskok*

Aerospace Engineering Department, Old Dominion University, Norfolk, Virginia 23529

We demonstrate negative dielectrophoresis (DEP) trapping of particles from high-conductivity media using a novel planar microelectrode that allows electrothermal enhancement of DEP traps. DEP force and electrothermal flow motion are investigated using a scaling analysis, numerical simulations, and experiments. Results show that the DEP trapping is enhanced by lateral transport of particles toward the capture zones due to electrothermal flow, whereas DEP trapping occurred only in limited spatial ranges without the flow motion. The electrothermally enhanced DEP will broaden the limit of electrokinetic manipulations in high-conductivity media. By providing patterned trapping zones that can act as target-specific attachment/detection sites, the presented device allows development of biosensor applications for rapid detection of pathogens and other microorganisms within a practical range of buffer conductivity.

Rapid and reliable detection of pathogens is of great importance in food safety, water and environmental monitoring, and clinical diagnosis. As a promising solution for continuous and real-time detection, several biosensors are being developed recently. The main advantages of the use of biosensors are low cost of analysis, the suitability to be miniaturized/integrated in automated assays, and the possibility of on-site/real-time analysis.[1,2] Most of biosensor technologies involve trapping of particles onto detection surfaces where specific recognition probes are immobilized (e.g., enzyme, nucleic acid, cell, antibody, molecularly imprinted polymer, etc.).[3] Effectiveness of the surface-based detection can be limited by low concentration of particles, and selective trapping of target species on probe surfaces becomes important to improve detection limit of biosensors. Trapping of target species can be done in a passive manner with diffusion-dominated transport, which occurs over relatively long time scales (order of hours). Thus, active manipulation techniques are required to achieve much shorter analysis time (order of minutes) and lower detection limit.[4]

Active control of colloidal motion can be achieved through the application of a variety of physical forces, including mechanical, fluidic, optical, acoustic, electrokinetic, and electromagnetic.[4] Among these forces, dielectrophoresis (DEP) has several advantages such as remote manipulation of particles by electric field control and simple configuration of devices without mechanical moving components.[5] DEP is the motion of polarizable particles that are suspended in an ionic solution and subjected to a spatially nonuniform electric field. When the polarizability of the particles is larger than that of the fluid, the particles move toward regions of the high electric field density (positive DEP). If the fluid is more polarizable than the particles, the particles move away from the high electric field density (negative DEP). It is possible to induce frequency-specific variations in particle polarizability using ac electric fields, which further enriches the realm of DEP applications.

Positive DEP has been utilized for trapping and separating colloidal particles by several researchers using interdigitated, grid, point-and-lid, and ring−dot electrode configurations.[6] Positive DEP is very effective for concentration of target species in low-conductivity media such as distilled water.[7,8] Magnitude of the positive DEP force quickly diminishes with increased medium conductivity, severely limiting its use for realistic applications. This issue is especially important for handling living microorganisms, since the use of low-conductivity buffers often results in high mortality rate of microorganisms due to an excessive osmotic stress.[9]

An alternative approach for trapping targets from a high-conductivity medium is utilizing negative DEP, which repels particles toward the local electric field minima. Several electrode designs that amplify the negative DEP are castellated, quadrupole, and microwell electrodes, based on two-dimensional geometries,[10−12] and insulator-based DEP, octopole, and patterned indium tin oxide (ITO) electrodes with three-dimensional configurations.[7,13−16]

* To whom correspondence should be addressed. Fax: 757-683-3200. Phone: 757-683-6818. E-mail: abeskok@odu.edu.

(1) Lazcka, O.; Campo, F. J. D.; Munoz, F. X. *Biosens. Bioelectron.* **2007**, *22*, 1205–1217.
(2) Palchetti, I.; Mascini, M. *Anal. Bioanal. Chem.* **2008**, *391*, 455–471.
(3) Rodriguez-Mozaz, S.; Marco, M.-P.; Lopez de Alda, M. J.; Barceló, D. *Anal. Bioanal. Chem.* **2004**, *378*, 588–598.
(4) Albrecht, D. R.; Sah, R. L.; Bhatia, S. N. *Biophys. J.* **2004**, *87*, 2131–2147.
(5) Gascoyne, P. R. C.; Vykoukal, J. *Electrophoresis* **2002**, *23*, 1973–1983.
(6) Voldman, J. *Annu. Rev. Biomed. Eng.* **2006**, *8*, 425–454.
(7) Lapizco-Encinas, B. H.; Simmons, B. A.; Cummings, E. B.; Fintschenko, Y. *Electrophoresis* **2004**, *25*, 1695–1704.
(8) Zhou, R.; Wang, P.; Chang, H.-C. *Electrophoresis* **2006**, *27*, 1376–1385.
(9) Aldaeus, F.; Lin, Y.; Roeraade, J.; Amberg, G. *Electrophoresis* **2005**, *26*, 4252–4259.
(10) Huang, Y.; Pethig, R. *Meas. Sci. Technol.* **1991**, *2*, 1142–1146.
(11) Pethig, R.; Huang, Y.; Wang, X. B.; Burt, J. P. H. *J. Phys. D: Appl. Phys.* **1992**, *25*, 881–888.
(12) Rosenthal, A.; Voldman, J. *Biophys. J.* **2005**, *88*, 2193–2205.
(13) Schnelle, T.; Mulller, T.; Fuhr, G. *J. Electrost.* **2000**, *50*, 17–29.
(14) Bhatt, K. H.; Grego, S.; Velev, O. D. *Langmuir* **2005**, *21*, 6603–6612.

10.1021/ac802471g CCC: $40.75
Published on Web 02/12/2009

Recently, capture of viruses suspended in 0.88 S/m physiological buffer using a quadrupole electrode was demonstrated.[17] However, this configuration requires four electrodes with opposite phases, and thus the repetition of electrode pattern to create multiple detection sites is difficult. Despite the urgent need for bioparticle manipulation for biomedical, environmental monitoring, and food-safety applications, direct DEP trapping and patterning of biological species from high-conductivity buffers (0.2 to 2 S/m) onto designated detection surfaces is limited.[18,19]

One limiting factor for the development of DEP traps in high-conductivity media is the lack of electrode design that allows simple fabrication, creation of multiple capture sites with strong trapping, and integration with sensor applications. Unlike positive DEP, particles are repelled from the electrodes' surfaces and transported to low electric field zones. Hence, well-defined local electric field minima are required for negative DEP traps. For surface-based biosensor applications, these electric field minima should be located at predefined multiple sensing sites on the bottom or top sides of the device.

Another important issue for DEP applications in high-conductivity media is the electrothermal flow motion. For the design of efficient DEP device that can manipulate biological samples within practical ranges of buffer conductivities, an electric field of sufficiently high intensity is generally required. Meanwhile, such an amplified electric field also interacts with the suspending media through ac-electroosmotic and electrothermal flow motions. Electrode polarization effects are negligible at high-frequency and high-conductivity ranges where negative DEP manipulation is effective, and thus ac electroosmosis is insignificant.[20] However, the effect of electrothermal motion becomes significant in the electrokinetic manipulation of high-conductivity samples because Joule heating depends on the magnitude of the electric field, as well as the conductivity of the media. Increased energy dissipation in the system causes local heating inside the fluid volume, and DEP force on particles is often overcome by the hydrodynamic drag force induced by the electrothermal motion of high-conductivity fluids. Thus, understanding the effects of electrothermal flow on DEP motion of particles is crucial for the development of high-conductivity sample applications.

In this paper, we present the design and development of a negative DEP based microfluidic device for trapping colloidal particles from high-conductivity media onto patterned surfaces, where target-specific probes can be implemented. The designed negative DEP trap is examined in a wide range of conductivities for manipulation of colloidal particles with known properties, and electrothermal effects on DEP trapping of particles in high-conductivity media are investigated. The objectives of this paper are the following:

(1) design of planar negative DEP traps that allow easy fabrication and strong particle trapping onto patterned surfaces in high-conductivity media;

(2) theoretical and numerical investigations of DEP effectiveness and electrothermal flow motion in various medium conductivities;

(3) experimental validation of the electrothermally enhanced negative DEP particle trapping.

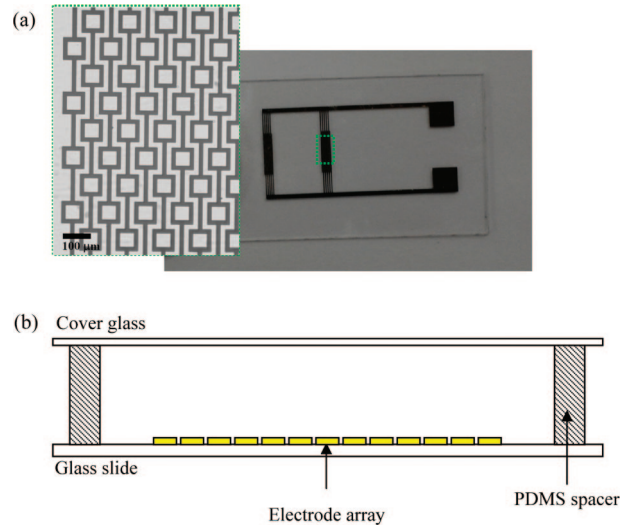

Figure 1. (a) Photograph of the gold electrode deposited on a microscope glass slide. (b) Schematic of the microfluidic chamber configuration.

METHODS AND MATERIALS

Electrode Geometry. We designed and fabricated simple planar square block electrodes as negative DEP traps. The electrodes consist of interdigitated positive and negative electrodes with repeated patterns of square blocks as shown in Figure 1a. Separation between the electrodes is kept constant at 20 μm. Each interdigitated electrode has square patterns with 60 μm × 60 μm inner area. An electric potential well is created inside these patterns isolated by strong electric field between the positive and negative electrodes. The symmetry of electrodes in both lateral and longitudinal directions is maintained with the repeated patterns to induce symmetric electrothermal flow motions above the electrodes. This configuration enables trapping of the colloidal particles at designed areas inside the square blocks on a planar surface, which enables integration with diagnostic devices. For example, the square patterns can be exploited for probe surfaces of specific antibodies and various kinds of biosensors. Optical, electrochemical, and piezoelectric biosensors[19] can be possibly integrated within the negative DEP traps to identify the target species. In addition, the negative DEP traps can be scaled up to create multiple capture sites by simply repeating the patterns due to the symmetric design. Planar electrodes require simple fabrication steps, giving our design a competitive advantage over other existing negative DEP trap designs.

Device Fabrication and Experiment. The designed electrodes were fabricated on microscope slides using conventional photolithographic techniques (see the Supporting Information). After attaching wires to the electrode ends, a fluid chamber (1.5 mm × 7 mm) was constructed by placing a 400 μm thick poly(dimethylsiloxane) (PDMS, Sylgard 184, Dow Corning) spacer

(15) Suzuki, M.; Yasukawa, T.; Mase, Y.; Oyamatsu, D.; Shiku, H.; Matsue, T. *Langmuir* **2004**, *20*, 11005–11011.
(16) Suzuki, M.; Yasukawa, T.; Shiku, H.; Matsue, T. *Langmuir* **2007**, *23*, 4088–4094.
(17) Docoslis, A.; Tercero Espinoza, L. A.; Zhang, B.; Cheng, L.-L.; Israel, B. A.; Alexandridis, P.; Abbott, N. L. *Langmuir* **2007**, *23*, 3840–3848.
(18) Lim, D. V.; Simpson, J. M.; Kearns, E. A.; Kramer, M. F. *Clin. Microbiol. Rev.* **2005**, *18*, 583–607.
(19) Stevens, K. A.; Jaykus, L.-A. *Crit. Rev. Microbiol.* **2004**, *30*, 7–24.
(20) Green, N. G.; Ramos, A.; Gonzalez, A.; Morgan, H.; Castellanos, A. *Phys. Rev. E* **2000**, *61*, 4011.

on the observation area, which was covered with a microscope cover glass during the experiments, as schematically shown in Figure 1b. Latex particles of 1 μm (IDC, Interfacial Dynamics) and silica particles of 1 μm (8100, Duke Scientific) were diluted with deionized (DI) water (Simplicity, Millipore), and the ionic concentration of the solution was adjusted by adding NaCl. Test solutions were prepared at three different conductivities: 1×10^{-5} S/m (DI water), 0.05 S/m (3.8 mM NaCl), and 0.224 S/m (17 mM NaCl). Each test solution was then pipetted into the fluid chamber, and a 10 V_{pp} ac voltage was supplied by a function generator (AFG 3102, Tektronix) at 10 MHz frequency.

Numerical Simulation. A commercially available software (CFD-ACE+, CFD Research Corp.) is used for the numerical simulation of electrothermal flow and the prediction of DEP force on the square block electrodes. Numerical formulation details can be found in the Supporting Information.

RESULTS AND DISCUSSION

Scaling Analysis. In a previous study, we reported a scaling analysis that can predict dominant particle transport mechanisms at a given electric field and material conditions.[21] Phase diagrams were demonstrated as a useful tool for understanding the relative contribution of the Brownian motion and ac electrokinetic forces including electrophoresis, DEP, and hydrodynamic forces due to the bulk fluid motion induced by ac electroosmosis. However, an explicit comparison with hydrodynamic force due to the electrothermal flow was not attempted. Electrothermal effects are essentially related with a characteristic length different from the electrode geometry, which is required to predict the order of magnitude of the circulatory flow motion.

In this section, we extend our scaling analysis to include electrothermal flow motions. Electrothermal flow refers to the fluid motion due to the spatial variation of electrical properties of a liquid medium, induced by the temperature gradients due to the Joule heating in presence of electric fields. With the assumption of negligible electrode polarization effects at high frequency, the maximum electrothermal flow velocity can be expressed as[22]

$$u_{\mathrm{ETH,max}} = \frac{1}{192\pi^2}\frac{M}{T}\frac{\varepsilon\sigma V^4}{k\mu r_{\mathrm{ETH}}} \tag{1}$$

where T is the temperature, ε is the electrical permittivity, σ is the electrical conductivity, V is the applied voltage, k is the thermal conductivity, μ is the viscosity, and r_{ETH} is the characteristic length for electrothermal flow. The electrothermal factor M is given by

$$M = \frac{(\beta - \alpha)T}{1 + (\omega\varepsilon/\sigma)^2} + \frac{1}{2}\alpha T \tag{2}$$

where ω is the radian frequency, $\alpha = (\partial\varepsilon/\partial T)/\varepsilon$, and $\beta = (\partial\sigma/\partial T)/\sigma$. For aqueous solutions with moderate concentration ($\sim$1 M), $\alpha = -0.0046$ K^{-1} and $\beta = 0.02$ K^{-1} can be used.[23] If the fluctuation of electrical properties inside the fluid is large, these relations cannot be applied and higher order terms for modeling the gradient of electrical properties should be included. The direction and magnitude of the electrothermal flow depend on the M factor, which is a strong function of the applied frequency. Theoretical investigation of the frequency dependence of the DEP force and the electrothermal flow motion is given in the Supporting Information.

From numerical studies, which will be discussed in the next section, it was observed that the electrothermal flow structure was not varying much with the medium conductivity if the sign of the M factor was kept unchanged. The radius of the counter-rotating flow rolls was calculated as 64 μm at 10 MHz frequency in 0.05 S/m liquid medium, and the flow rolls with a similar size (64.5 μm) but increased magnitude of velocity was numerically predicted for 0.224 S/m medium conductivity. Additional test cases with different applied voltages at 0.224 S/m conductivity also confirmed that the flow structure was maintained and only the magnitude of flow velocity was varied proportional to the fourth power of the applied voltage ($u_{\mathrm{ETH,max}} \sim 24$, 376, and 6100 μm/s for $V = 5$, 10, and 20 V), which is consistent with the analytical prediction in eq 1. We modeled the characteristic length scale of the electrothermal flow, r_{ETH}, as the radius of this flow roll based on the simple theoretical expression in a two-dimensional system.[24] The estimation of the maximum electrothermal flow velocity using the scaling analysis showed a good agreement with numerical results. The characteristic length scale for the electrothermal flow is comparable to the electrode pattern length of 60 μm, which is measured from the gap between two opposite electrodes to the center of the square pattern. Since the fluid chamber height is assumed large compared with the electrode pattern length, the periodic flow structure is mainly dependent on the electrode configuration. However, the characteristic length scale for the electrothermal flow will differ from the electrode pattern length, if the chamber height becomes comparable to the pattern length.

Using the characteristic length scale for modeling the electrothermal flow motion, we modified the scaling analysis and generated phase diagrams. Figure 2 shows the phase diagram for variations of dominant forces and magnitude of the DEP transport. Latex particle of 1 μm was modeled with parameters $\varepsilon_p = 2.55$, $\sigma_p = 0.01$ S/m, $\varepsilon = 78.5$, $V = 10$ V_{pp}, $a = 0.5$ μm, and characteristic lengths for the electric field and the electrothermal flow were $r = 10$ μm and $r_{\mathrm{ETH}} = 65$ μm, respectively. Frequency and conductivity values that correspond to the experimental conditions are specified on each plot with stars (10 MHz for 1×10^{-5}, 0.05, and 0.224 S/m). It can be seen in Figure 2a that negative DEP motion is dominant with respect to other forces only at certain frequency and conductivity ranges. At 10 MHz frequency, negative DEP can be utilized in 1×10^{-5} and 0.05 S/m liquid media as expected from the DEP spectra (Figure S2a in the Supporting Information). However, electrothermal motion is dominant over negative DEP at the increased conductivity of 0.224 S/m. Figure 2b shows the variation of magnitude of the DEP motion as a function of the frequency and medium conductivity for fixed voltage and characteristic length. The negative DEP displacement of particles is not changing much

(21) Park, S.; Beskok, A. *Anal. Chem.* **2008**, *80*, 2832–2841.
(22) Ramos, A.; Morgan, H.; Green, N. G.; Castellanos, A. *J. Phys. D: Appl. Phys.* **1998**, *31*, 2338–2353.
(23) Lide, D. R. *CRC Handbook of Chemistry and Physics*, 74th ed.; CRC Press: London, 1994.
(24) Castellanos, A.; Ramos, A.; Gonzalez, A.; Green, N. G.; Morgan, H. *J. Phys. D: Appl. Phys.* **2003**, *36*, 2584–2597.

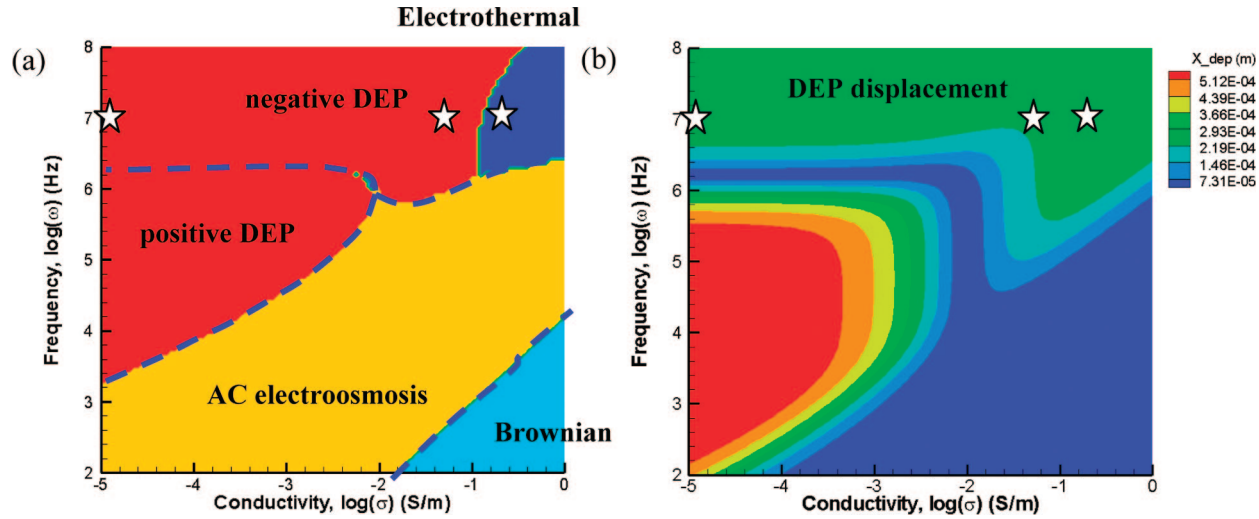

Figure 2. (a) Frequency−conductivity phase diagram. (b) Particle displacement (per second) due to the DEP force. A latex particle of 1 μm is modeled with the following parameters: $\varepsilon_p = 2.55$, $\sigma_p = 0.01$ S/m, $\varepsilon = 78.5$, $V = 10$ V_{pp}; characteristic lengths for electric field and electrothermal flow are $r = 10$ μm and $r_{ETH} = 65$ μm, respectively. Frequency and conductivity values that correspond to the experimental condition are specified on each plot with stars (10 MHz for 1×10^{-5}, 0.05, and 0.224 S/m).

and remaining at the same order of magnitude for high-frequency (>10 MHz) or high-conductivity (>0.1 S/m) ranges, where Re{K} approaches its minimum value of −0.5. Thus, the variation of DEP forces on particles for different medium conductivities is insignificant. Instead, electrothermal effects are amplified as the medium conductivity increases, and the negative DEP can be overcome by the electrothermal flows as predicted in the phase diagram.

Numerical Results. The quasi-static electric field and the temperature distribution inside the fluid volume are presented in the Supporting Information (Figure S3). The resultant nonuniform electric field induces DEP forces acting on suspended particles. Figure 3a shows the DEP force distribution at the plane 10 μm above the electrode surface. Contour colors represent direction of the vertical component of DEP force, while vectors show the horizontal components of the DEP force. The lateral components of DEP force vector show that particles will be driven to the trapping zones. Resultant DEP forces for three different medium conductivities are similar because the values of Re{K} are close to −0.5 at 10 MHz frequency.

Figure 3b shows the effect of the electrothermal flow motion on the DEP trapping. The isosurface represents the effective DEP trapping zone determined by the direction of the vertical component of the DEP force. Inside the volume enclosed by this surface, the DEP force pushes particles onto the bottom surface. Effects of the electrothermal fluid motion can be seen clearly from the flow velocity distribution plotted in the same figure. Main flow circulations on the square pattern can be observed on each symmetry plane, which merge at the center of the trapping zone and induce vertical flow motion. At the electrode gaps on the y−z symmetry plane, counter vortices due to the main flow circulation are generated, creating complex local flows. For the conductivity of 0.05 S/m, the maximum velocity of the flow is calculated as 55 μm/s. In the case of a higher medium conductivity (0.224 S/m), the flow structure was similar and the maximum electrothermal flow velocity was 376 μm/s. The flow direction was reversed in the case of DI water (1×10^{-5} S/m) as predicted by the electrothermal spectra (Figure S2b in the Supporting Information). However, the velocity magnitude in DI water was very small ($\sim 10^{-3}$ μm/s) and the electrothermal effects were negligible. A pair of counter-rotating flow rolls has been reported in the literature as a typical electrothermal flow structure on planar interdigitated electrodes in two-dimensional simulations.[25−27] Since the width of the presented electrode is smaller than the length of its straight portion, similar flow structure is locally observed in the vicinity between the two parallel electrodes at the y−z symmetry plane. However, two counter vortices with different sizes and strengths are achieved due to the asymmetry between the positive and negative electrodes, and the flow pattern is dominated by the larger flow roll on the square electrodes. Since each pattern is surrounded with counter electrodes with a constant separation distance, these flow rolls are expected to occur along the sides of the square shape except near the interconnects of the square patterns. A single vortex is observed at the x−z symmetry plane above the interconnects. These main circulation regions generate lateral fluid motion toward the center of the DEP traps around the square patterns.

The flow rolls along the sides of the square electrode create the lateral fluid motion toward the center of the trapping zone, and the particles are expected to be continuously transported to the DEP zones by hydrodynamic forces of the flow. Thus, the induced electrothermal flow in the presented device is anticipated to enhance DEP trapping. Since particles initially residing outside of the trapping ranges can be brought to DEP zones by the circulatory fluid motion, DEP trapping is expected to increase by time. At the same time, trapping of particles on capture sites requires the dominance of the DEP force over hydrodynamic drag due to the vertical electrothermal flow motions inside the DEP zones. The electrothermal flow velocity decreases rapidly near the stagnation zone on the bottom surface, where DEP trapping is expected to be always effective. However, the vertical flow

(25) Chen, D. F.; Du, H. *J. Micromech. Microeng.* **2006**, *16*, 2411–2419.
(26) Feldman, H. C.; Sigurdson, M.; Meinhart, C. D. *Lab Chip* **2007**, *7*, 1553–1559.
(27) Sigurdson, M.; Wang, D.; Meinhart, C. D. *Lab Chip* **2005**, *5*, 1366–1373.

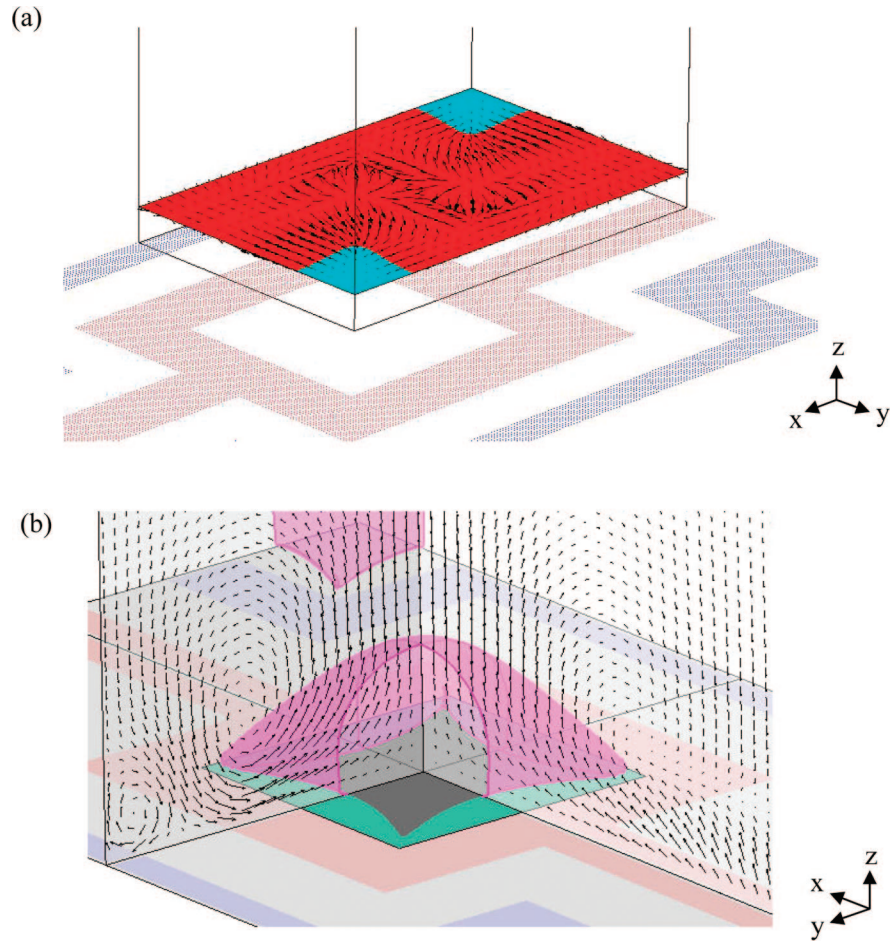

Figure 3. (a) DEP force direction acting on 1 μm latex particles at 10 V_{pp} voltage and 10 MHz frequency. The planar components of DEP forces are plotted at a plane 10 μm above the electrode surface (vectors). Contour colors represent the direction of the vertical component of the DEP force (red—upward, cyan—downward). (b) Electrothermal flow velocity distribution at the symmetry planes. Effective DEP trapping zone is determined by the direction of the vertical component of the DEP force, represented with the isosurface. Inside this zone, the DEP force pushes particles onto the bottom surface.

velocity increases gradually and reaches a maximum value approximately 40 μm above the surface. DEP trapping becomes less effective away from the bottom surface, while the hydrodynamic drag due to the electrothermal flow motion increases. As the medium conductivity is increased, the electrothermal flow motion amplifies and the DEP transport can be overcome by the flow motion over ~0.1 S/m as predicted in the scaling analysis. Thus, it can be expected that particle trapping near the stagnation zones will be enhanced because of the flow circulation in high-conductivity media. However, the trapping enhancement can be reduced above the stagnation zones as the electrothermal flow motion dominates DEP transport and circulates more particles out of the effective DEP zones along the vertical flow stream.

Experimental Results. Negative DEP trapping of particles on the presented electrodes was experimentally observed with suspensions of 1 μm latex particles. Figure 4 shows the trapping results of the latex particles suspended in media with three different conductivities, 1×10^{-5} S/m (DI water), 0.05 S/m (3.8 mM NaCl), and 0.224 S/m (17 mM NaCl). Images were taken after applying 10 V_{pp} ac electric field at 10 MHz for 5 and 30 min. Trapping of the latex particles onto designed square patterns from DI water is shown in Figure 4a. Particles were captured inside the DEP traps at 5 min, but noticeable increase of DEP trapping was not observed at 30 min. As predicted in the scaling analysis and the numerical simulations, electrothermal flow motion was negligible for 1×10^{-5} S/m, and the continuous circulation of particles by the fluid motion could not be achieved. Sedimentation of latex particles was insignificant because the characteristic velocity for the gravitational motion of latex particles (specific gravity 1.05) was negligible, which was estimated using the force balance with Stokes drag for small particles as $u_g = (2/9)ga^2(\rho_p - \rho)/\eta = 0.027$ μm/s. Thus, the concentration of trapped particles was not increased by time.

Figure 4b shows particle trapping from 0.05 S/m medium. In comparison with the DI water case, more particles were trapped inside the square patterns at 5 min and a considerable increase of particle trapping was observed at 30 min. Since DEP force variation due to the increase of the medium conductivity is negligible at 10 MHz operating frequency, increased concentration of trapped particles at 5 and 30 min can be explained with the continuous lateral transport of particles toward DEP zones by the electrothermal flow motion as predicted in the numerical simulations. This DEP trapping enhancement by the lateral motion of electrothermal flow was still observed in 0.224 S/m medium, as shown in Figure 4c. In comparison with the DI water case where the transport of particles by the flow motion was negligible, more particles were trapped inside the capture zones at 5 min and

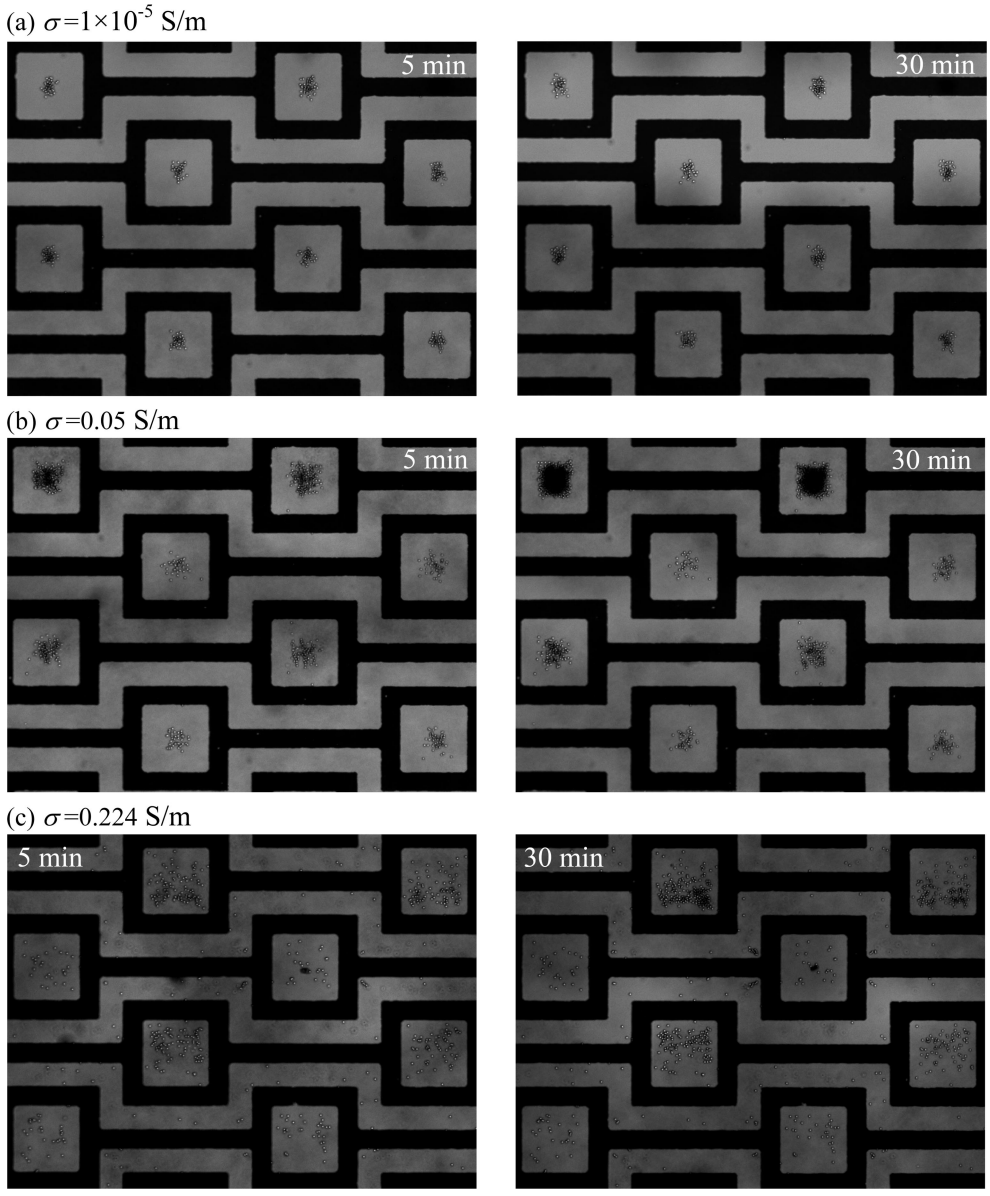

Figure 4. Images of 1 μm latex particles suspended in (a) DI water (1×10^{-5} S/m), (b) 3.8 mM NaCl solution (0.05 S/m), and (c) 17 mM NaCl solution (0.224 S/m) after applying an ac electric field for 5 and 30 min at 10 V_{pp} voltage and 10 MHz frequency.

increase of particle concentration was observed at 30 min. However, the increase of particle concentration inside the capture zones between 5 and 30 min was not as substantial, when compared with the case of 0.05 S/m. In this case, the lateral transport of particles toward DEP zones by the flow motion further increases, but the vertical flow velocity that circulates particles out of the DEP zones is also increasing. Thus, more particles can escape from the DEP zones along the flow stream as the electrothermal flow becomes dominant over DEP forces.

In order to observe the effects of the lateral electrothermal flow motion more clearly, silica particles suspended in the same ionic solutions (1×10^{-5}, 0.05, and 0.224 S/m) were tested. Variation of the DEP force due to different medium conductivities was negligible because the real part of the CM factor for silica particles was almost a constant ($\mathrm{Re}\{K\} \approx -0.5$). Figure 5 shows trapped silica particles after applying 10 V_{pp} ac electric field at 10 MHz frequency for 5 and 30 min. The particles were captured inside the DEP traps from DI water at 5 min, and the concentration of trapped particles increased by time because of particle sedimentation, as shown in Figure 5a. The characteristic velocity for the gravitational motion of silica particles (specific gravity 2.2) was estimated as $u_g = 0.65$ μm/s.

Figure 5b shows trapping of particles in 0.05 S/m medium. The electrothermal effects increased the particle concentration inside the DEP traps at 5 and 30 min compared with the case of DI water. At the same time, sedimentation of silica particles, which occurred on the experimental time scale ($l/u_g \sim 10^3$ s), assisted particle trapping. But the vertical electrothermal flow motion limited the particle sedimentation because the gravitational transport of the particles in this case was locally overcome by the flow motion ($u_{ETH,max} \sim 55$ μm/s). Figure 5c shows similar results obtained from 0.224 S/m particle solution. The concentration of trapped particles was increased at 5 min compared with cases a and b because of increased lateral transport of particles

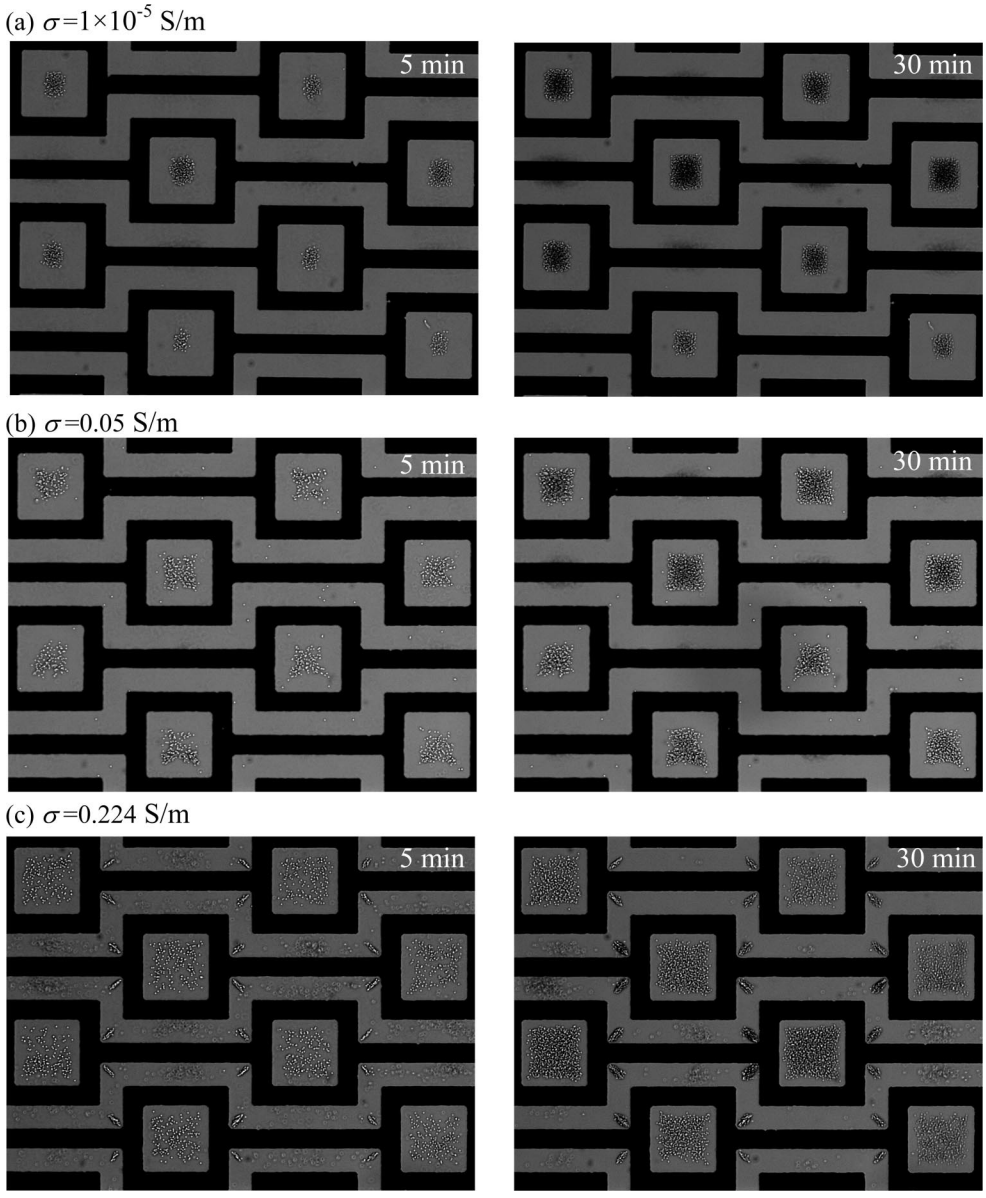

Figure 5. Images of 1 μm silica particles suspended in (a) DI water (1 × 10^{-5} S/m), (b) 3.8 mM NaCl solution (0.05 S/m), and (c) 17 mM NaCl solution (0.224 S/m) after applying an ac electric field for 5 and 30 min at 10 V_{pp} voltage and 10 MHz frequency.

by the flow motion and DEP capture inside the stagnation zones. However, the amplified electrothermal flow motion became dominant over DEP forces inside DEP zones, and the trapping efficiency above the stagnation zones was reduced. Accordingly, the particle concentration inside the square patterns increased more gradually compared with case b. In addition, it can be seen that some particles were trapped near the corner of the square patterns, where secondary electric field minima exist. Because the electrostatic shielding due to the electric double layer on the bottom surface decreases as the ionic concentration is increased, particles near the surface could be bound more easily. Partial modification of the electrode design will be required to minimize effects of the secondary electric field minima to reduce trapping of particles around these corner zones.

Numerical simulations and experiments demonstrate that particle trapping was enhanced by the lateral transport of particles toward DEP traps due to the electrothermal flow. However, the trapping efficiency can be reduced as the electrothermal effects are further amplified to be dominant over DEP. It can be conjectured that the optimal condition for the electrothermal enhancement would exist, which is related with the hydrodynamic and DEP forces on the trapping zones. The relative magnitude of each transport mechanism can be predicted by the scaling analysis, and operational parameters can be estimated in an early design stage. However, the optimization of the device geometry (r_{ETH}) for the maximum trapping efficiency will require detailed analysis and correlation.

The presented study considers various parameters for the prediction of the DEP trap performance with a theoretical framework. Thus, this approach can be extended to other specific biological species with established modeling parameters. For example, based on the model of *Clostridium sporogenes* bacterial spores in our previous study,[21] we successfully applied a similar approach for trapping of the bacterial spores in apple juice and milk, which have conductivities of 0.224 and 0.524 S/m, respectively (Figure S4 in the Supporting Information).

CONCLUSIONS

Negative DEP trapping of particles from high-conductivity media is demonstrated using a novel planar microelectrode that allows electrothermal enhancement of DEP traps. Scaling analysis was utilized to predict the conductivity (>0.1 S/m) and frequency (>10 MHz) ranges where DEP transport can be overcome by the electrothermal motion. Numerical simulations and experiments demonstrated that particle trapping was enhanced by the lateral transport of particles toward DEP traps due to the electrothermal flow, whereas DEP trapping occurred only in limited spatial ranges without the flow motion. The trapping enhancement can be reduced if the electrothermal flow motion dominates DEP transport and circulates particles out of the effective DEP zones. Future studies include optimization of the DEP capture unit by reducing the circulating flow inside DEP zones. In addition, the presented electrode has well-defined electric field minima that can act as target-specific attachment/detection sites. Integration of diagnostic devices within these capture sites may enable rapid detection of pathogens and other microorganisms in high-conductivity media.

ACKNOWLEDGMENT

This research was supported by the U.S. Department of Homeland Security (Grant No. N-00014-04-1-0659), through a Grant awarded to the National Center for Food Protection and Defense at the University of Minnesota. Any opinions, findings, conclusions, or recommendations expressed in this publication are those of the author(s) and do not represent the policy or position of the Department of Homeland Security.

SUPPORTING INFORMATION AVAILABLE

Additional information as noted in text. This material is available free of charge via the Internet at http://pubs.acs.org.

Received for review November 21, 2008. Accepted January 22, 2009.

AC802471G